

Tropical–Extratropical Interactions with the MJO Skeleton and Climatological Mean Flow

SHENGQIAN CHEN

Department of Mathematics, University of Wisconsin–Madison, Madison, Wisconsin

ANDREW J. MAJDA

Department of Mathematics, and Center for Atmosphere Ocean Science, Courant Institute of Mathematical Sciences, New York University, New York, New York

SAMUEL N. STECHMANN

Department of Mathematics, and Department of Atmospheric and Oceanic Sciences, University of Wisconsin–Madison, Madison, Wisconsin

(Manuscript received 28 January 2016, in final form 18 July 2016)

ABSTRACT

Simplified asymptotic models are developed to investigate tropical–extratropical interactions. Two kinds of interactions are illustrated in the model: (i) MJO initiation through extraction of energy from barotropic Rossby waves and (ii) MJO termination via energy transfer to extratropical Rossby waves. A new feature, in comparison to previous simplified models, is that here these waves interact directly in the presence of a climatological mean flow given by the Walker circulation. The simplified models are systems of ordinary differential equations (ODEs) for the amplitudes of barotropic Rossby waves and the MJO, and they are systematically derived from the MJO skeleton model by using multiscale asymptotics. The simplified ODEs allow for rapid investigation of a wide range of model parameters, such as initial conditions and wind shear. Zonally uniform wind shear is shown to have only a minor effect on these interactions here, in contrast to the important role of the zonally varying wind shear associated with the Walker circulation. The models illustrate some realistic features of tropical–extratropical interactions on intraseasonal to seasonal time scales. A key aspect of the models here is that the water vapor and convective activities are interactive components of the model, rather than specified external heating sources.

1. Introduction

The Madden–Julian oscillation (MJO) is the dominant component of intraseasonal (≈ 30 – 60 days) variability in the tropics (Madden and Julian 1971, 1972, 1994). It is an equatorial wave envelope of complex multiscale convective processes, coupled with planetary-scale ($\approx 10\,000$ – $40\,000$ km) circulation anomalies. Individual MJO events propagate eastward at a speed of roughly 5 m s^{-1} , and their convective signal is most prominent over the Indian and western Pacific Oceans (Zhang 2005). In addition to its significance in its own right, the MJO also significantly

affects many other components of the atmosphere–ocean–Earth system, such as monsoon development, intraseasonal predictability in midlatitudes, and the development of El Niño–Southern Oscillation (ENSO) (Lau and Waliser 2012; Zhang 2005, 2013).

Besides its strong tropical signal, the MJO interacts with the global flow on the intraseasonal time scales. Teleconnection patterns between the global extratropics and the MJO have been described in early observational analyses by Weickmann (1983), Weickmann et al. (1985), and Liebmann and Hartmann (1984). Their results demonstrate coherent fluctuations between extratropical flow and eastward-propagating outgoing longwave radiation (OLR) anomalies in the tropics. In a later study, Matthews and Kiladis (1999) illustrate the interplay between high-frequency transient extratropical waves and the MJO. More recently, Weickmann and Berry (2009)

Corresponding author address: Shengqian Chen, Department of Mathematics, University of Wisconsin–Madison, 480 Lincoln Dr., Madison, WI 53706.
E-mail: sqchen@math.wisc.edu

demonstrate that convection in the MJO frequently evolves together with a portion of the activity in a global wind oscillation. Gloeckler and Roundy (2013) argued by using lagged composite analysis that the high-amplitude extratropical circulation pattern is associated with simultaneous occurrence of both the MJO and the equatorial Rossby wave events.

Besides observational analyses, models have also been used to study the interactions between the MJO and extratropical waves. By including tropical convection forcing data in a barotropic model, Ferranti et al. (1990) found significant improvement in the model's predictability. Hoskins and Ambrizzi (1993) argued from their model that a zonally varying basic state is necessary for the MJO to excite extratropical waves by forcing perturbations to a barotropic model. To view the extratropical response to convective heating, Jin and Hoskins (1995) forced a primitive equation model with a fixed heat source in the tropics in the presence of a climatological background flow and obtained the Rossby wave train response as a result. To diagnose the specific response to patterns of convection like those of the observed MJO, Matthews et al. (2004) forced a primitive equation model in a climatological background flow with patterns of observed MJO. The resulting global response to that heating is similar in many respects to the observational analysis. The MJO initiation in response to extratropical waves was illustrated by Ray and Zhang (2010). They show that a dry-channel model of the tropical atmosphere developed MJO-like signals in tropical wind fields when forced by reanalysis fields at poleward boundaries. In addition, Lin et al. (2009) showed the significance of midlatitude dynamics in triggering tropical intraseasonal response by including extratropical disturbances in a tropical circulation model. Frederiksen and Frederiksen (1993) used a two-level primitive equation eigenvalue model and found large-scale basic-state flow and cumulus heating to be necessary for generating MJO modes with realistic structures. Many other interesting studies on tropical–extratropical interactions have been carried out. For example, see the review by Roundy (2011).

Among the past studies based on climate models, typically the effect of the MJO is represented by forced perturbations (Hoskins and Ambrizzi 1993; Jin and Hoskins 1995; Matthews et al. 2004), or the influences of the midlatitude variations are treated as boundary effects for the tropical circulation model (Ray and Zhang 2010; Lin et al. 2009; Frederiksen and Frederiksen 1993; Roundy 2011). Such simplifications are useful for isolating individual processes within these complex models. As a next step, it would be desirable to design a simplified model where both the MJO and extratropical

waves are simultaneously interactive, rather than externally imposing one of these two components; such an approach was recently taken by Chen et al. (2015), as described next.

Chen et al. (2015) developed a simplified model that includes both the MJO and tropical–extratropical interactions. Specifically, this model combines (i) the interactions of the dry barotropic mode and first baroclinic mode, which have been studied by Majda and Biello (2003) and Khouider and Majda (2005), with (ii) the MJO skeleton model of Majda and Stechmann (2009, 2011). The MJO skeleton model includes the interactive dynamics of moisture q and convective activity envelope a . It has captured the main features of the MJO at the intraseasonal/planetary scale: (i) the slow phase speed of $\approx 5 \text{ m s}^{-1}$; (ii) the peculiar dispersion relation of $d\omega/dk \approx 0$; and (iii) the horizontal quadrupole vortex structure. By combining the barotropic equations and the MJO skeleton, the model of Chen et al. (2015) illustrated applications to MJO initiation and termination, including three-wave interaction cases of (i) interaction of the MJO, equatorial baroclinic Rossby waves, and barotropic Rossby waves; and (ii) interaction of the MJO, baroclinic Kelvin waves, and barotropic Rossby waves. In those cases, the barotropic Rossby wave acts like a catalyst for the interaction between the MJO and dry equatorial waves, but its own amplitude is nearly unchanged. One of the main purposes of the present paper is to investigate scenarios in which the barotropic Rossby waves may significantly exchange energy with the MJO. Two possible factors are wind shear and sea surface temperature (SST) variations and the accompanying variations in the climatological tropical circulation, the Walker circulation (Webster 1972, 1981, 1982; Hoskins and Jin 1991; Majda and Biello 2003). The present work will investigate the effects of regional varying SST and global shear flow in the interactions between the MJO and barotropic Rossby waves. It will be seen that the presence of the Walker circulation allows significant energy exchanges between barotropic Rossby waves and the MJO.

Last, it is worth noting that, for an investigation of MJO initiation and termination such as the present study, the MJO skeleton model has several important properties that make it an appropriate choice of model. First, the MJO skeleton model has been shown to reproduce the initiation and termination of wave trains of two to three MJO events in succession (Thual et al. 2014), similar to MJO events in nature (Yoneyama et al. 2013). Second, the MJO skeleton model reproduces statistics of MJO events, such as the number and duration of events, that are similar to the statistics of MJO events in nature (Stachnik et al. 2015). These aspects of

MJO events are in addition to the MJO's more basic features; in particular, the MJO skeleton model predicts the speed and structure of the MJO (Majda and Stechmann 2009, 2011; Thual and Majda 2015, 2016).

The paper is organized as follows. Section 2 describes the barotropic–first baroclinic MJO skeleton model, including SST regional variations and the resulting Walker circulation. Unbalanced moisture and cooling source terms with spatial variations are taken into account in the MJO skeleton to represent the effect of SST, in which case the Walker circulation can be found as the steady-state solution of the baroclinic system. The energy principle and asymptotic expansions are also presented. In section 3, the resonance condition is identified in the presence of an idealized Walker circulation, which mediates the interaction between the MJO and the barotropic Rossby waves. Two cases are numerically computed for the ODE system: (i) MJO initiation and (ii) MJO termination and excitation of barotropic Rossby waves. Section 4 considers more general Walker circulation cases composed of two different wavenumbers. New ODE systems are derived for the resonant condition, and numerical results are presented. Section 5 investigates the effect of a zonally uniform shear flow. Finally, section 6 is a concluding discussion.

2. Model description

a. The barotropic–first baroclinic MJO skeleton model

The barotropic–first baroclinic β -plane equations with water vapor and convection can be written as

$$\frac{\partial \bar{\mathbf{v}}}{\partial t} + \bar{\mathbf{v}} \cdot \nabla \bar{\mathbf{v}} + y \bar{\mathbf{v}}^\perp + \nabla \bar{p} = -\frac{1}{2} \nabla \cdot (\mathbf{v} \otimes \mathbf{v}), \quad (1a)$$

$$\nabla \cdot \bar{\mathbf{v}} = 0, \quad (1b)$$

for the barotropic mode and

$$\frac{\partial \mathbf{v}}{\partial t} + \bar{\mathbf{v}} \cdot \nabla \mathbf{v} - \nabla \theta + y \mathbf{v}^\perp = -\mathbf{v} \cdot \nabla \bar{\mathbf{v}}, \quad (1c)$$

$$\frac{\partial \theta}{\partial t} + \bar{\mathbf{v}} \cdot \nabla \theta - \nabla \cdot \mathbf{v} = \delta^2 (\bar{H}a - S^\theta), \quad (1d)$$

$$\frac{\partial q}{\partial t} + \bar{\mathbf{v}} \cdot \nabla q + \tilde{Q} \nabla \cdot \mathbf{v} = -\delta^2 (\bar{H}a - S^q), \quad (1e)$$

$$\frac{\partial a}{\partial t} + \bar{\mathbf{v}} \cdot \nabla a = \Gamma qa. \quad (1f)$$

for the first baroclinic mode. These equations combine the MJO skeleton model (Majda and Stechmann 2009) and nonlinear interactions between the baroclinic and barotropic modes (Majda and Biello 2003). The details of this model are described in Chen et al. (2015). Here,

$\bar{\mathbf{v}} = (\bar{u}, \bar{v})$, $\bar{\mathbf{v}}^\perp = (\bar{v}, -\bar{u})$ and \bar{p} are barotropic velocity and pressure, respectively. The barotropic streamfunction ψ can be used to rewrite (1a) and (1b) as

$$\frac{\partial}{\partial t} \Delta \bar{\psi} + \bar{\mathbf{v}} \cdot \nabla \Delta \bar{\psi} + \psi_x + \frac{1}{2} \nabla \cdot [-(\mathbf{v}u)_y + (\mathbf{v}v)_x] = 0. \quad (2)$$

The other variables, $\mathbf{v} = (u, v)$ and θ are baroclinic velocity and potential temperature; and q is water vapor (sometimes referred to as ‘‘moisture’’). The coefficients \bar{H} and \tilde{Q} are prefactors to give $\bar{H}a$ the units of a heating rate and a vertical moisture gradient parameter, respectively. The tropical convective activity envelope is denoted by $\delta^2 a$, where δ is a small parameter that modulates the scales of the tropical convection envelope. We define δ^2 as the ratio of radiative cooling rate of 1 K day^{-1} divided by the reference heating rate scale at 10 K day^{-1} . Likewise, δ^2 is also incorporated with the radiative cooling and the moisture sources, S^θ and S^q . Here, for simplicity, we consider $\delta^2 S^\theta$ and $\delta^2 S^q$ to be spatially varying and time independent, although, in general, they have both spatial and temporal variations.

b. Walker circulation and energy evolution

First, consider the baroclinic system (1c)–(1f) with the barotropic velocity ignored. When the system has unbalanced moistening and cooling sources (i.e., $S^q \neq S^\theta$), the Walker circulation is formed for the baroclinic equations with zero barotropic winds. When $\bar{\mathbf{v}} = 0$, the Walker circulation is the steady-state solution for the baroclinic system (Ogrosky and Stechmann 2015):

$$-\nabla \theta_w + y \mathbf{v}_w^\perp = 0, \quad (3a)$$

$$\nabla \cdot \mathbf{v}_w = \delta^2 \frac{S^\theta - S^q}{1 - \tilde{Q}}, \quad (3b)$$

$$q_w = 0, \quad (3c)$$

$$a_w = \frac{S^q - \tilde{Q} S^\theta}{\bar{H}(1 - \tilde{Q})}. \quad (3d)$$

When the Walker circulation variables are subtracted from the baroclinic variables, the baroclinic system has energy conservation for the anomalies: $d\mathcal{E}_{\text{BCa}}/dt = 0$, where

$$\begin{aligned} \mathcal{E}_{\text{BCa}} = & \frac{1}{2} \int_{-Y}^Y \int_0^X \frac{1}{2} [|\mathbf{v} - \mathbf{v}_w|^2 + (\theta - \theta_w)^2] \\ & + \frac{1}{\tilde{Q}(1 - \tilde{Q})} [q + \tilde{Q}(\theta - \theta_w)]^2 \\ & + \frac{\delta^2}{\tilde{Q}\Gamma} [\bar{H}a - a_w \log(a)] dx dy. \end{aligned} \quad (4)$$

Now consider the full coupled system (1), including both the barotropic and baroclinic components. When the barotropic energy $\mathcal{E}_{\text{BT}} = (1/2) \int_{-Y}^Y \int_0^X |\bar{\mathbf{v}}|^2 dx dy$

is also considered, the total energy for the anomalies is $\mathcal{E} = \mathcal{E}_{\text{BCa}} + \mathcal{E}_{\text{BT}}$, and it evolves according to the following:

$$\begin{aligned} \frac{d\mathcal{E}}{dt} = & -\frac{1}{2} \int_{-Y}^Y \int_0^X \bar{\mathbf{v}} \cdot \nabla [\mathbf{v}_W \otimes \mathbf{v}_W + (\mathbf{v} - \mathbf{v}_W) \otimes \mathbf{v}_W + \mathbf{v}_W \otimes (\mathbf{v} - \mathbf{v}_W)] \\ & + (\mathbf{v} - \mathbf{v}_W) \cdot (\mathbf{v}_W \cdot \nabla \bar{\mathbf{v}} + \bar{\mathbf{v}} \cdot \nabla \mathbf{v}_W) + [\tilde{Q}q + (1 + \tilde{Q}^2)(\theta - \theta_W)] \bar{\mathbf{v}} \cdot \nabla \theta_W dx dy. \end{aligned} \quad (5)$$

Note that the right-hand side of this equation depends on the strength of the Walker circulation, and in general it is not zero, so the energy is not conserved. The Walker circulation here behaves as an energy source/sink for the MJO mode and the barotropic Rossby wave.

c. Asymptotic ansatz

The asymptotic expansion is now carried out by introducing equatorial long-wave scaling,

$$x' = \delta x, \quad t' = \delta t, \quad \text{and} \quad v' = \frac{1}{\delta} v, \quad (6)$$

as well as the longer time scales:

$$T_1 = \delta t', \quad T_2 = \delta^2 t'. \quad (7)$$

Hence, in the asymptotic model, three long time scales are involved: t' , T_1 , and T_2 . Their characteristic time scales are 1, 3, and 10 days, respectively. In addition, small-amplitude variables are also assumed for asymptotic expansion:

$$\begin{aligned} (\psi, u, v', \theta, q) = & \delta^2 (\psi_1, u_1, v_1, \theta_1, q_1) + \delta^3 (\psi_2, u_2, v_2, \theta_2, q_2) \\ & + \delta^4 (\psi_3, u_3, v_3, \theta_3, q_3) + O(\delta^5), \end{aligned} \quad (8a)$$

$$a = \bar{a} + \delta a_1 + \delta^2 a_2 + \delta^3 a_3 + O(\delta^4), \quad (8b)$$

where each of the variables on the right-hand side of (8) is a function of x' , t' , T_1 , and T_2 , although this dependence has been suppressed in (8) to ease notation. For the moisture source and radiative cooling, it is assumed that

$$S^q = \bar{S}^q + \delta S_1^q, \quad S^\theta = \bar{S}^\theta + \delta S_1^\theta, \quad (9)$$

where $\overline{(\dots)} = \int (\dots) dx dy$ is the mean value over the horizontal domain. We further assume that $\bar{S}^q = \bar{S}^\theta = \bar{H} \bar{a}$, which is a necessary consistency condition to ensure the existence of a steady Walker circulation (Majda and Klein 2003).

Under this assumption for S^q and S^θ , the Walker circulation would only appear in the leading order, so the

baroclinic variables at the leading order can be written as follows:

$$\begin{aligned} (u_1, v_1, \theta_1, q_1, a_1) = & (u_1, v_1, \theta_1, q_1, a_1)_W \\ & + (u_1, v_1, \theta_1, q_1, a_1)_a, \end{aligned} \quad (10)$$

where the subscript W stands for Walker circulations, and the subscript a stands for the leading-order anomalies from the Walker circulation.

d. Meridional basis truncation

To carry out the multiscale analysis, a meridional truncated basis is used for all of the variables. The main reason for introducing a meridional truncation is that the linear eigenmodes of (1) are not known, whereas the linear eigenmodes of a truncated version of this system are known and were previously described by Majda and Stechmann (2009). We adopt the same meridional structure described in Chen et al. (2015), and the barotropic wind is assumed as

$$\psi(x, y, t) = B(x, t) \sin(Ly), \quad (11)$$

where L is the meridional wavenumber. For the baroclinic variables, the meridional structures are assumed to be

$$l(x, y, t) = l^{(0)}(x, t) \Phi_0(y) + l^{(2)}(x, t) \Phi_2(y), \quad (12a)$$

$$r(x, y, t) = r^{(0)}(x, t) \Phi_0(y) + r^{(2)}(x, t) \Phi_2(y), \quad (12b)$$

$$v(x, y, t) = v^{(1)}(x, t) \Phi_1(y), \quad (12c)$$

$$q(x, y, t) = q^{(0)}(x, t) \Phi_0(y) + q^{(2)}(x, t) \Phi_2(y), \quad (12d)$$

$$\bar{H} a(x, y, t) - S^\theta(x, y, t) = \bar{H} a^{(0)}(x, t) \Phi_0(y), \quad (12e)$$

where $l = -(u + \theta)/2$ and $r = (u - \theta)/2$ are the Riemann invariants for the baroclinic system, and $\Phi(y)$ are the parabolic cylinder functions. The motivation for this particular truncation is mainly to have the simplest system that includes the Kelvin wave and the first symmetric equatorial Rossby wave; see Chen et al. (2015) for further discussion. The details of the parabolic cylinder functions can be found in the appendix. In addition, we

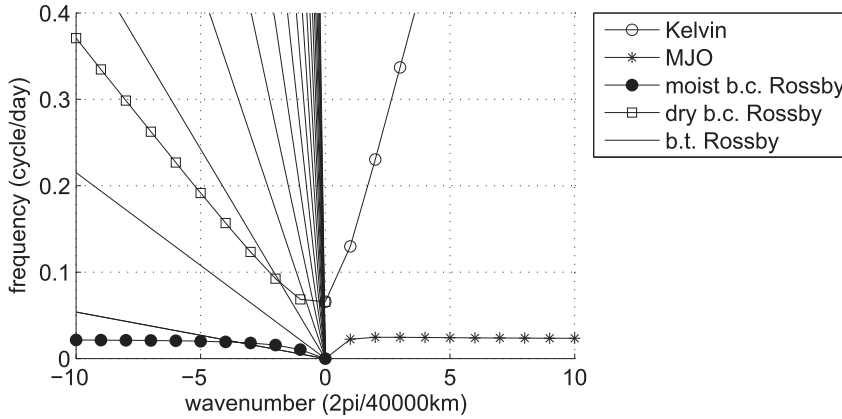


FIG. 1. Dispersion relation for linear waves. The dispersion curve of the Kelvin mode is denoted with open circles, the MJO with asterisks, the moist baroclinic Rossby mode with closed circles, the dry baroclinic Rossby mode with squares, and the barotropic Rossby mode with no symbols.

also assume that the variations for moisture source and radiative cooling share the same zonal structure:

$$S_1^q = \tilde{S}^{qy}(y)\tilde{S}^x(x), \quad S_1^\theta = \tilde{S}^{\theta y}(y)\tilde{S}^x(x), \quad (13)$$

although in general they often have different zonal structures. Further, the meridional structures are assumed to be proportional to the leading parabolic cylinder function:

$$\tilde{S}^{qy}(y) = c_q \Phi_0(y), \quad \tilde{S}^{\theta y}(y) = c_\theta \Phi_0(y), \quad (14)$$

The asymptotic expansions in (8) are then applied to the meridional truncated system, which is described in the appendix. At the leading order, the truncated system is linear, and the baroclinic and barotropic systems are decoupled. The four major eigenmodes for the baroclinic system were described in Majda and Stechmann (2009), and they are the Kelvin, MJO, moist Rossby, and dry Rossby modes, as shown in Fig. 1.

3. Direct tropical–extratropical interaction mediated by Walker circulation

This section provides the reduced ODE model that includes direct tropical–extratropical interactions mediated by the Walker circulation. In particular, numerical computations for two cases will be given for this interaction mechanism: (i) MJO initiation and (ii) MJO termination and excitation of barotropic Rossby waves.

a. The reduced model

For the interaction of the MJO and barotropic Rossby wave, in the presence of the Walker circulation, their wavenumbers and frequencies must satisfy the resonance condition (Majda 2003):

$$k_{\text{MJO}} + k_W + k_T = 0, \quad (15a)$$

$$\omega_{\text{MJO}} + \omega_T = 0, \quad (15b)$$

where k_{MJO} , k_W , and k_T are the wavenumbers for the MJO, the Walker circulation, and the barotropic Rossby wave, respectively; and ω_{MJO} and ω_T are the wave frequencies for the MJO and the barotropic Rossby wave, respectively. The frequency for the Walker circulation ω_W is zero. This type of resonance condition is analogous to topographic resonance (Majda et al. 1999); the Walker circulation here plays an analogous role to the effect of topography. Because the MJO and barotropic Rossby waves travel in opposite directions, (15) implies that the wavenumber of the Walker circulation has to satisfy the following condition:

$$|k_W| \geq 2.$$

A Walker circulation with wavenumber $k_W = 2$ can be viewed in Fig. 2. One can view this wavenumber-2 Walker circulation as an idealization of the two main circulation cells in nature, which are centered over the Maritime Continent and South America (Stechmann and Ogrosky 2014; Ogrosky and Stechmann 2015). The resonance condition with $k_{\text{MJO}} = 1$ and $k_T = 1$ is shown in Fig. 3.

To proceed with the multiscale analysis, we write the leading-order baroclinic solution as

$$\mathbf{U}_1 = \alpha(T_1, T_2)e^{i(k_{\text{MJO}}x' - \omega_{\text{MJO}}t')} \mathbf{r}_{\text{MJO}} + e^{i(k_W x')} \mathbf{r}_W + \text{C.C.}, \quad (16)$$

and the leading-order barotropic solution as

$$B_1 = \frac{1}{\sqrt{2\pi L}} \beta(T_1, T_2)e^{i(k_T x' - \omega_T t')} + \text{C.C.}, \quad (17)$$

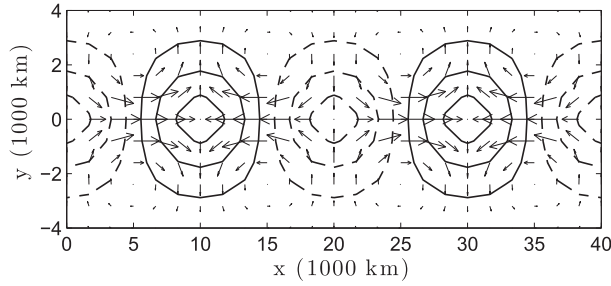


FIG. 2. Walker circulation with wavenumber $k_W = 2$. The contours denote the convective activity $\overline{H}a$, with positive (negative) anomalies denoted by solid (dashed) contours and with the zero contour removed. The contour interval is equal to one-fourth of the maximum value of $\overline{H}a$. The vectors denote the horizontal velocity field at the lower troposphere.

where C.C. stands for the complex conjugate, \mathbf{r}_{MJO} is the right eigenvector for the MJO mode, and \mathbf{r}_W is the right eigenvector of the Walker circulation. The eigenvector for the MJO mode is normalized by the baroclinic energy, as described by [Stechmann and Majda \(2015\)](#).

Next, the second- and third-order systems are considered in order to determine the evolution of $\alpha(T_1, T_2)$ and $\beta(T_1, T_2)$ from (16) and (17) on the long time scales T_1 and T_2 . A systematic multiscale asymptotic analysis is carried out to ensure the sublinear growth of the second- and third-order terms of the asymptotic expansion in (8). Following similar procedures as in [Chen et al. \(2015\)](#), the result is a reduced ODE model for the amplitudes of the modes:

$$\partial_{T_2} \beta + id_2 \beta + h_3 \alpha^* = 0, \quad (18a)$$

$$\partial_{T_2} \alpha + id_4 \alpha^2 \alpha^* + id_5 \alpha + h_6 \beta^* = 0, \quad (18b)$$

where coefficients d and h are shown in [Table 1](#) and are pure real values, and where the asterisk denotes complex conjugate. Three groups of interacting terms appear in this ODE system: the cubic self-interaction term $id_4 \alpha^2 \alpha^*$ corresponding to the nonlinear q - a interaction, the linear self-interaction terms $id_2 \beta$ and $id_5 \alpha$ related to dispersive terms in the barotropic–baroclinic system, and the coupled linear terms $h_3 \alpha^*$ and $h_6 \beta^*$ related to the Walker circulation. The coefficients d and h are from the procedure of multiscale asymptotic analysis. In contrast to the ODE system derived by [Chen et al. \(2015\)](#), in which the coupling terms are quadratic, here the coupling terms $h_3 \alpha^*$ and $h_6 \beta^*$ are linear. This is because the Walker circulation is involved in this coupling, but it is a stationary mode with fixed amplitude, so one part of the quadratic term is a fixed value.

The values of h_3 and h_6 in (18) are determined by the strength of the variations in the source terms, S_1^q and S_1^q , or their meridional projection coefficients, c_q and c_θ ,

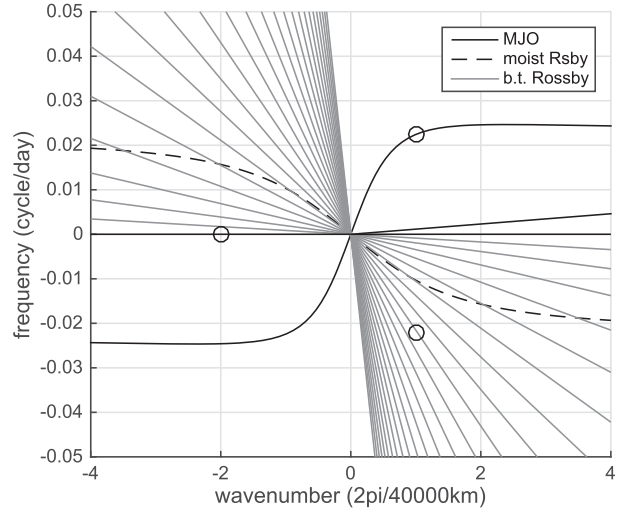


FIG. 3. Resonance condition for the interaction of the MJO, Walker circulation, and barotropic Rossby wave with wavenumbers $k_{\text{MJO}} = 1$, $k_W = -2$, and $k_T = 1$ as described in (15).

from (14). In this paper, for simplicity, the two coefficients are fixed so that $c_q = 1.2$ and $c_\theta = 1$, which results in the Walker circulation shown in [Fig. 2](#).

According to (18), the coupled linear terms determine the energy exchange between the two modes:

$$\frac{d|\alpha|^2}{dT_2} = -2h_3 \text{Re}(\alpha\beta), \quad \frac{d|\beta|^2}{dT_2} = -2h_6 \text{Re}(\alpha\beta), \quad (19)$$

where Re denotes the real part. At the leading order, the total energy E for the anomalies is

$$E = |\alpha|^2 + |\beta|^2, \quad (20)$$

which is only conserved when $h_3 + h_6 = 0$. However, this is generally not the case. In the computations carried out in this study, the coefficients h_3 and h_6 have opposite signs, indicating from (19) that as one mode is gaining energy, the other one is losing energy, but the total energy is not necessarily constant.

Here the simplified asymptotic equations in (18) are utilized to gain insight into the interactions between the MJO and the barotropic Rossby waves. For this purpose, the reduced model is integrated numerically for two sets of initial data: (i) MJO initiation: $\alpha|_{T_2=0} = 0$ and $\beta|_{T_2=0} = 1$; and (ii) MJO termination and excitation of barotropic Rossby waves: $\alpha|_{T_2=0} = 1$ and $\beta|_{T_2=0} = 0$. The computation time is up to 200 days to observe the properties of the solutions on the long T_2 time scale. A

TABLE 1. Coefficients in (18).

d_2	h_3	d_4	d_5	h_6
-0.0053	-0.1261	-0.0519	0.0017	0.4132

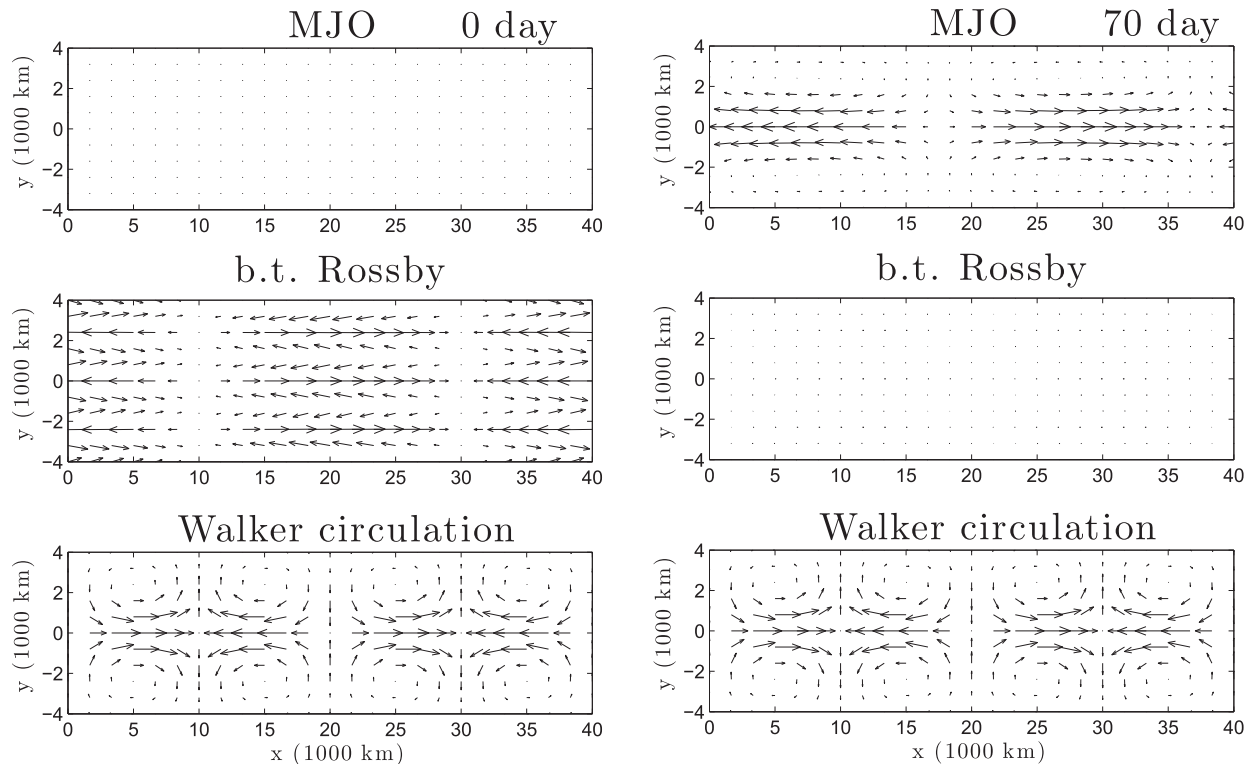


FIG. 6. Velocity field (lower tropospheric) of three modes for the case of MJO initiation at (left) 0 and (right) 70 days: (top) MJO; (middle) barotropic Rossby wave; and (bottom) Walker circulation.

the velocity field is zero at 0 days and achieves its maximum at 70 days. The barotropic Rossby wave is at its maximum initially and achieves its smallest magnitude at 70 days.

What determines the 140-day time scale for initiation and decay of a wave train of MJO events in the model? This time scale is related to the energy transfer between the MJO and barotropic Rossby waves. In (18), the coupling terms between the MJO and barotropic Rossby waves have coefficients of h_3 and h_6 , and therefore one expects h_3 and h_6 to play a key role in determining the time scale of energy exchange. [Note that the other terms in (18) can also contribute to the energy exchange time scale; their role is implicitly included in (19) in the $\text{Re}(\alpha\beta)$ factor.] Based on linear theory, if we linearize system (18) around $(\alpha, \beta) = (0, 0)$, the nondimensional time scale can be written as

$$T_{\text{osci}} = \frac{2\pi}{\delta^3 \sqrt{(d_2 + d_5)^2 - 4h_3h_6}}. \quad (21)$$

In the above expression, because h_3 and h_6 usually have opposite signs, the value inside the square root is usually positive. With plugging the coefficient values in Table 1, the dimensional time scale is 147 days, similar to the nonlinear time scale of ≈ 140 days seen in Figs. 4 and 5.

c. MJO termination and excitation of barotropic Rossby waves

To consider MJO termination and the excitation of barotropic Rossby waves, the initial condition is set to be $\alpha|_{T_2=0} = 1$ and $\beta|_{T_2=0} = 0$. Figure 7 shows the numerical simulation from the ODE solver. Similar to the MJO initiation case, the MJO mode and the barotropic Rossby waves are exchanging energy. The oscillation cycle is similar to MJO initiation at around 140 days. Different from the MJO initiation case, the MJO is losing energy, whereas the barotropic Rossby wave is gaining energy at 0 days, and the total energy of these two modes is decaying at first, until ≈ 70 days. The amplitudes and energy return to their original state at around 140 days.

4. More general Walker circulation

In the previous section, the case for the sinusoidal Walker circulation with wavenumber $k_W = 2$ is discussed. The realistic Walker circulation, on the other hand, is composed of a variety of wavenumbers. For example, Ogrosky and Stechmann (2015) described simplified versions of the Walker circulation using one or three Fourier modes in their study. In this section, another mode for the Walker cell, $k_W = 3$, is included in addition to

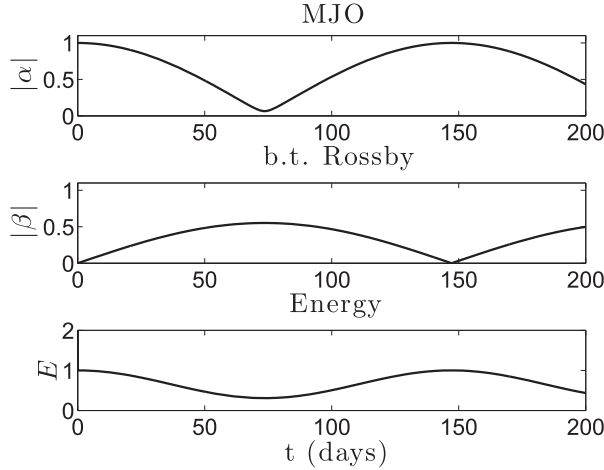


FIG. 7. As in Fig. 4, but with initial conditions corresponding to the case of MJO termination and excitation of barotropic Rossby waves.

$k_W = 2$. The Walker circulation in this case is shown in Fig. 8. In this situation, two sets of resonant triads arise corresponding with the two Walker cell wavenumbers:

$$k_{\text{MJO}1} + k_{W1} + k_{T1} = 0, \quad (22a)$$

$$\omega_{\text{MJO}1} + \omega_{T1} = 0, \quad (22b)$$

and

$$k_{\text{MJO}2} + k_{W2} + k_{T2} = 0, \quad (23a)$$

$$\omega_{\text{MJO}2} + \omega_{T2} = 0, \quad (23b)$$

where $k_{W1} = -2$ and $k_{W2} = -3$. The other wavenumbers are selected in the following way. To go along with these Walker cell wavenumbers, we consider standard wavenumbers 1 and 2 for the MJO, and then we select barotropic Rossby wavenumbers that complete the resonance conditions in (22) and (23). One could also imagine other reasonable choices, such as wavenumber 3, for the MJO, but we will restrict attention to wavenumbers 1 and 2 here as some initial reasonable choices for illustration. More specifically, the values for $k_{\text{MJO}1}$ and k_{T1} are both fixed to be 1, and two cases are considered: (i) $k_{\text{MJO}2} = 1$ and $k_{T2} = 2$; and (ii) $k_{\text{MJO}2} = 2$ and $k_{T2} = 1$. For case (i), $k_{\text{MJO}1}$ and $k_{\text{MJO}2}$ represent the same $k = 1$ MJO mode. For case (ii), k_{T1} and k_{T2} are the same wavenumber, but they represent barotropic Rossby waves with different meridional wavelengths. In the two cases below, the strengths of S_1^{θ} and S_1^q at wavenumber $k = 3$ are also chosen to be $c_q = 1.2$ and $c_{\theta} = 1$, as in the previous section, for simplicity, although more general situations can be applied.

a. Single MJO interacting with two barotropic waves

Here, three modes are considered: the MJO mode with wavenumber $k_{\text{MJO}1} = 1$ and barotropic Rossby

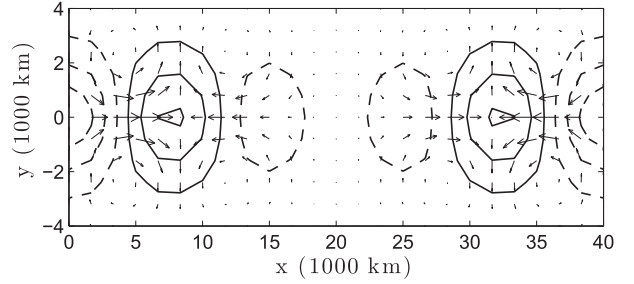


FIG. 8. As in Fig. 2, but for a Walker circulation with wavenumbers $k_W = 2$ and 3 as described in section 4.

waves with $k_{T1} = 1$ and $k_{T2} = 2$. The resonance conditions for the three modes are shown in Fig. 9. Here, the barotropic waves have two different meridional wavenumbers, L_1 and L_2 , so that the initial condition for the barotropic streamfunction can be written as

$$\begin{aligned} \psi_1 = & \delta^2 \sin(L_1 y) \frac{\beta_1}{\sqrt{2\pi L_1}} e^{i(k_{T1} x' - \omega_{T1} t')} \\ & + \delta^2 \sin(L_2 y) \frac{\beta_2}{\sqrt{2\pi L_2}} e^{i(k_{T2} x' - \omega_{T2} t')} + \text{C.C.}, \end{aligned} \quad (24)$$

where β_1 and β_2 are the amplitudes for the two barotropic Rossby waves. The initial condition for the baroclinic system is

$$\mathbf{U}_1 = \alpha(T_1, T_2) e^{i(k_{\text{MJO}} x' - \omega_{\text{MJO}} t')} \mathbf{r}_{\text{MJO}} + \mathbf{r}_{W1} + \mathbf{r}_{W2} + \text{C.C.}, \quad (25)$$

where \mathbf{r}_{W1} and \mathbf{r}_{W2} are the Walker circulation components at wavenumbers $k_W = 2$ and 3. These two resonant triads lead to the reduced ODE system:

$$\partial_{T_2} \beta_1 + id_{21} \beta_1 + h_{31} \alpha^* = 0, \quad (26a)$$

$$\partial_{T_2} \beta_2 + id_{22} \beta_2 + h_{32} \alpha^* = 0, \quad (26b)$$

$$\partial_{T_2} \alpha + id_4 \alpha^2 \alpha^* + id_5 \alpha + h_{61} \beta_1^* + h_{62} \beta_2^* = 0, \quad (26c)$$

where coefficients d and h are shown in Table 2. The derivation, not shown here, is similar to Chen et al. (2015). From system (26), we can see that both barotropic waves interact with the MJO mode α , but there is no direct interaction between the two barotropic Rossby waves β_1 and β_2 .

In principle, either one of the barotropic waves can potentially initiate the MJO. To consider each wave separately, two cases are computed numerically: (i) $\alpha|_{T_2=0} = 0$, $\beta_1|_{T_2=0} = 1$, and $\beta_2|_{T_2=0} = 0$; and (ii) $\alpha|_{T_2=0} = 0$, $\beta_1|_{T_2=0} = 0$, and $\beta_2|_{T_2=0} = 1$. Furthermore, additional cases, such as investigations of MJO termination, were also carried out. The results, not shown here, demonstrate that the energy is exchanged mainly between the MJO and the barotropic Rossby wave with $k_T = 1$, whereas the

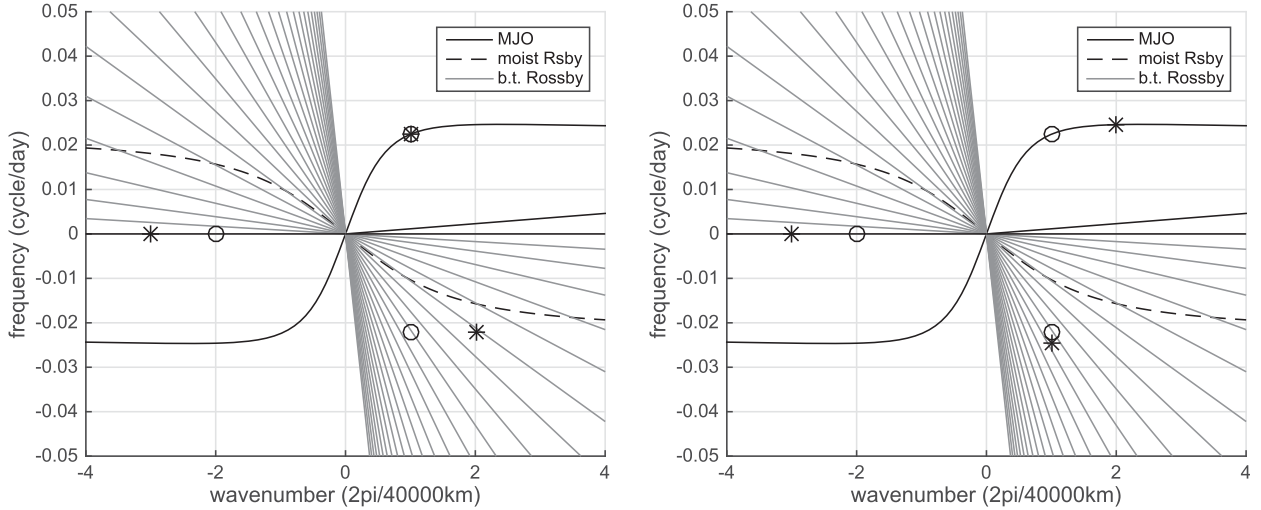


FIG. 9. Resonance conditions in (22) and (23) with more realistic Walker circulation. (left) One MJO mode interacting with two barotropic Rossby waves as in section 4a; (right) two MJO modes interacting with two barotropic Rossby waves as in section 4b. Open circles correspond with (22) and asterisks correspond with (23).

wavenumber $k_T = 2$ Rossby wave (which has meridional wavelength of $2\pi/L_2 \approx 840$ km) exchanges only a very small amount of energy with the MJO.

b. Two MJO modes interacting with two barotropic Rossby waves

In this section, four modes are considered: the MJO modes with wavenumbers $k_{\text{MJO}1} = 1$ and $k_{\text{MJO}2} = 2$ and two barotropic Rossby waves with the same zonal wavenumbers $k_{T1} = k_{T2} = 1$ but different meridional wavenumbers L_1 and L_2 . Figure 9 (right) shows the resonance condition for the interactions between the

four modes. The ansatz for the barotropic wind can still be written as (24), and

$$\begin{aligned} \mathbf{U}_1 = & \alpha_1(T_1, T_2) e^{i(k_{\text{MJO}1}x' - \omega_{\text{MJO}1}t')} \mathbf{r}_{\text{MJO}1} \\ & + \alpha_2(T_1, T_2) e^{i(k_{\text{MJO}2}x' - \omega_{\text{MJO}2}t')} \mathbf{r}_{\text{MJO}2} + \mathbf{r}_{W1} + \mathbf{r}_{W2} + \text{C.C.} \end{aligned} \quad (27)$$

for the baroclinic modes, where α_1 and α_2 stand for amplitudes for the MJO at wavenumbers $k_{\text{MJO}1} = 1$ and $k_{\text{MJO}2} = 2$. The following coupled ODE system describes the interaction mechanism:

$$\partial_{T_2} \beta_1 + id_{21} \beta_1 + h_{31} \alpha_1^* = 0, \quad (28a)$$

$$\partial_{T_2} \alpha_1 + id_{41} \alpha_1^2 \alpha_1^* + ig_1 \alpha_1 \alpha_2 \alpha_2^* + id_{51} \alpha_1 + h_{61} \beta_1^* = 0, \quad (28b)$$

$$\partial_{T_2} \beta_2 + id_{22} \beta_2 + h_{32} \alpha_2^* = 0, \quad \text{and} \quad (28c)$$

$$\partial_{T_2} \alpha_2 + id_{42} \alpha_2^2 \alpha_2^* + ig_2 \alpha_2 \alpha_1 \alpha_1^* + id_{52} \alpha_2 + h_{62} \beta_2^* = 0, \quad (28d)$$

where coefficients d and h are shown in Table 3. Again, the derivation, not shown here, is similar to Chen et al. (2015). In this ODE system, besides the existing coupled

linear terms between the MJO–barotropic Rossby wave interactions, additional cubic interactions appear between the two MJO modes. Specifically, the terms for

TABLE 2. Coefficients in (26).

d_{21}	h_{31}	d_{22}	h_{32}	d_4	d_5	h_{61}	h_{62}
−0.0053	−0.0630	−0.0106	0.0060	−0.0519	0.0017	0.2066	−0.0158

TABLE 3. Coefficients in (28).

d_{21}	h_{31}	d_{22}	h_{32}	d_{41}	g_1	d_{51}	h_{61}	d_{42}	g_2	d_{52}	h_{62}
-0.0053	-0.1261	-0.0064	-0.0959	-0.0519	-0.0375	0.0017	0.4132	-0.0984	-0.1503	0.0044	0.3960

MJO–MJO interactions are $ig_1\alpha_1\alpha_2\alpha_2^*$ in (28b) and $ig_2\alpha_2\alpha_1\alpha_1^*$ in (28d). These cubic interactions arise from the nonlinear q – a interaction in the MJO skeleton model, similar to the cubic self-interaction terms in Chen et al. (2015).

Figure 10 shows the MJO initiation with initial conditions $\alpha_1|_{T_2=0} = \alpha_2|_{T_2=0} = 0$ and $\beta_1|_{T_2=0} = \beta_2|_{T_2=0} = 1$. It can be seen from the reduced system (28) that the barotropic Rossby waves β_1 and β_2 are necessary to initiate MJO modes α_1 and α_2 , respectively. In Fig. 10, the two MJO modes interact with each other, and the solutions do not follow a periodic pattern. Also, notice that the MJO is significantly weakened for times 110–140 days, but it is not completely terminated. To illustrate this more clearly, Fig. 11 is the Hovmöller diagram for the convective envelope of the leading-order MJO waves with wavenumbers 1 and 2. A wave packet is presented in the diagram with a life cycle around 150 days. These cases illustrate that incorporating more realistic zonal variation into the Walker circulation yields more realistic zonal variation of the MJO (Ogrosky and Stechmann 2015).

Note that the Hovmöller diagram in Fig. 11 displays a westward group velocity, which occurs here in the presence of the Walker circulation. This westward group velocity has also been documented in cases without extratropical wave interactions (Majda and Stechmann 2011), in the presence of a warm pool, and it is also consistent with observational analyses of the MJO, as seen in Hendon and Salby (1994) and Adames and Kim (2016). In a more idealized setting with a zonally uniform base state (Majda and Stechmann 2011), the MJO skeleton model instead displays an eastward group velocity at some wavelengths.

5. Effects of wind shear

This section includes the effect of the horizontal and vertical wind shear in the model. In the past, dry models (Webster 1972, 1981, 1982; Hoskins and Jin 1991; Majda and Biello 2003) suggest that wind shear can significantly affect energy transfer between the barotropic waves and tropical waves. Both zonally uniform and

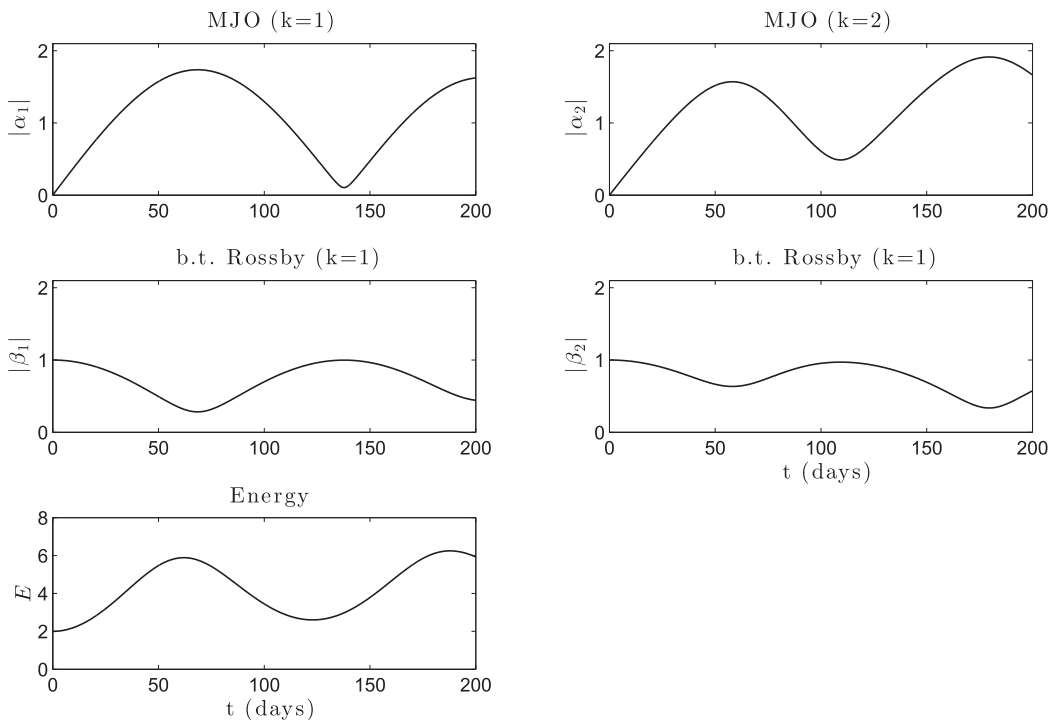


FIG. 10. Solution of the reduced model (28) for the case of MJO initiations with two MJO modes: $k_{MJO1} = 1$ and $k_{MJO2} = 2$, as described in section 4b.

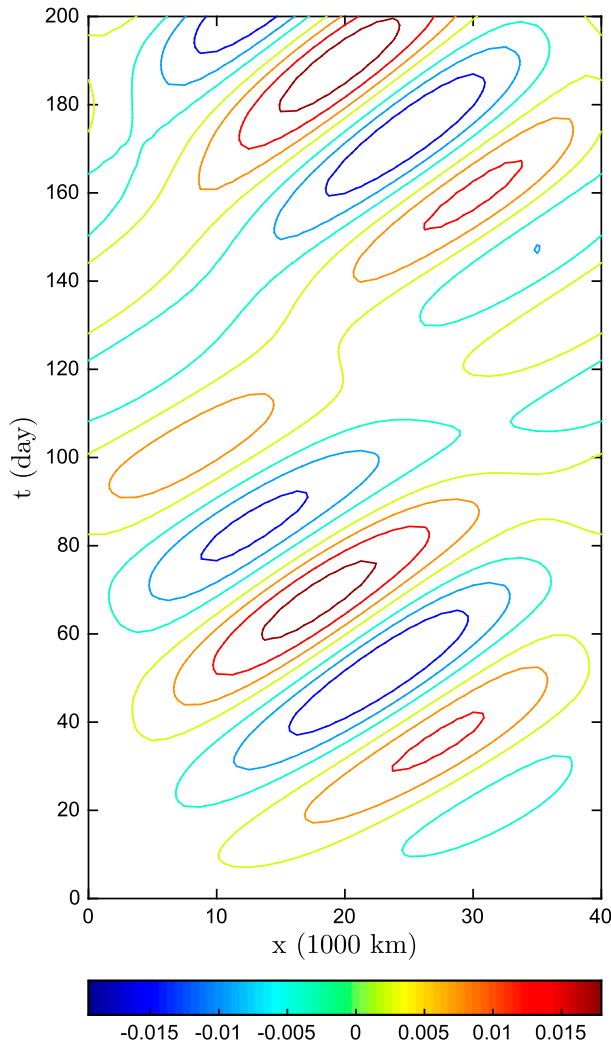


FIG. 11. Hovmöller diagram of $\bar{H}a_{10}$ for MJO initiation with two MJO modes: $k_{\text{MJO1}} = 1$ and $k_{\text{MJO2}} = 2$, as described in section 4b.

zonally varying wind shear have been considered in these past studies. However, the MJO, water vapor, and convective activity were not explicitly included in these models. Motivated by previous studies, here we consider both barotropic and baroclinic wind shear that is $O(\delta^2)$:

$$[\tilde{u}(x, y, z), \tilde{v}(x, y, z), \tilde{w}(x, y, z)] = [\tilde{U}(y, z), 0, 0], \quad (29)$$

where

$$\begin{aligned} \tilde{U}(y, z) = & \delta^2 [U_0 + L \sin(Ly)B_0 \\ & + \cos(\pi z)(u_0^{(0)}\Phi_0 + u_0^{(2)}\Phi_2)]. \end{aligned} \quad (30)$$

Here, U_0 is the constant global mean flow, B_0 is the strength of the barotropic wind shear in the meridional direction, and $u_0^{(0)}$ and $u_0^{(2)}$ are the strengths of the baroclinic wind shear in the first two symmetric meridional

TABLE 4. Coefficients in (31).

d_2	h_3	d_4	d_5	h_6
-0.0053	-0.1261	-0.0519	0.0017	0.4132

basis functions. Note that we consider only zonally uniform wind shear in the present study; it would be interesting to consider a zonally varying barotropic wind shear in the future.

A similar multiscale analysis is carried out, and the resonance condition is not affected by the wind shear. The reduced ODE model for the MJO–barotropic Rossby wave interaction is:

$$\partial_{T_2}\beta + i(d_2 + f_1)\beta + h_3\alpha^* = 0, \quad (31a)$$

$$\partial_{T_2}\alpha + id_4\alpha^2\alpha^* + i(d_5 + f_2)\alpha + h_6\beta^* = 0, \quad (31b)$$

where coefficients d , f , and h when $U_0 = B_0 = 1$ are shown in Table 4. The wind shear introduces two additional linear terms with coefficients f_1 and f_2 , both of which are real values. In the derivation of (31), only the effect of baroclinic shear arises. In order for the baroclinic shear to have an effect, it must instead be assumed to have an amplitude of $O(\delta)$; in such a case (not shown), the inclusion of the baroclinic shear also introduces similar self-interacting linear terms so that the reduced ODE is in the same form as (31) in any case.

Numerical simulations are performed for MJO initiation with the effects of barotropic shear. The resonance condition is the same as in section 3. Four different barotropic shear profiles are considered: (i) $U_0 = 0$ and $B_0 = 1$; (ii) $U_0 = -1$ and $B_0 = 1$; (iii) $U_0 = 1$ and $B_0 = 0$; and (iv) $U_0 = 1$ and $B_0 = 1$. The results for the four cases (not shown here) suggest that the barotropic shear has little effect on the maximum amplitude attained by MJO and the time period of the solution. The small effect of wind shear here differs from the important effects of wind shear seen by Majda and Biello (2003), and several differences in the models could contribute to the different results. In particular, in the model of Majda and Biello (2003), the waves are all nondispersive; resonant interactions are included for all wavenumbers rather than a small discrete subset of wavenumbers; and moisture and convection are not explicitly included.

6. Concluding discussion

Asymptotic models have been designed and analyzed here for the nonlinear interaction between the MJO and the barotropic Rossby waves. The models involve the combination of the barotropic and equatorial baroclinic modes together with interactive moisture and convective

activity envelopes. An important feature of this framework is that the tropical and extratropical dynamics are interactive, whereas other models commonly specify one of these components as an external forcing term or boundary condition.

In the presence of the Walker circulation, the MJO and the barotropic Rossby waves can interact directly. In section 3, the reduced ODE model is derived by identifying resonant triads that include the MJO, the Walker circulation, and the barotropic Rossby wave. Two cases are presented: (i) MJO initiation and (ii) MJO termination and excitation of barotropic Rossby waves. In contrast to the results in Chen et al. (2015), in which the barotropic Rossby wave exchanges very little energy with other modes, here the barotropic Rossby wave and the MJO exchange energy directly. The time period between initiation and termination is about 140 days, depending on spatial location; this is a realistic time scale, since the MJO's oscillation period is 30–60 days and MJO events commonly appear as wave trains of two or three successive events (Yoneyama et al. 2013; Thual et al. 2014; Stachnik et al. 2015).

To explore more realistic conditions, Walker circulations were also considered with more general zonal variations. Multiple resonant triads are identified to generate energy exchange between different modes. In particular, a four-wave MJO–MJO–barotropic Rossby–barotropic Rossby interaction is found with MJO at wavenumbers 1 and 2, in which the two MJO modes interact through the nonlinear coupling term between moisture and convective activity envelope in the MJO skeleton equation. In this case, rather than an idealized MJO with a single zonal wavenumber, a wave packet of MJO events arises with an amplitude that is zonally localized.

As a final element of additional realism considered here, horizontal and vertical shear were incorporated in the model. The barotropic and baroclinic shear, if zonally uniform, have little effect on the energy exchange between the MJO and the barotropic Rossby waves. This is in contrast to the significant effect of zonally varying wind shear as part of the Walker circulation. Further investigations are needed to better understand the role of wind shear in these different settings.

Besides the MJO skeleton model used here, other models of the MJO are also in use. For example, the MJO is described as a “moisture mode” by Sobel and Maloney (2013) and Adames and Kim (2016), and other models by Yang and Ingersoll (2013) are formulated without moisture. One could use these models to carry out a study of tropical–extratropical interactions. Here, the MJO skeleton model was used for several reasons. For instance, the MJO skeleton model predicts the

speed and structure of the MJO (Majda and Stechmann 2009, 2011; Chen and Stechmann 2016) and also its vertical tilts (Thual and Majda 2015, 2016). Furthermore, it has been shown to reproduce the initiation and termination of wave trains of two to three MJO events in succession (Thual et al. 2014), similar to MJO events in nature (Yoneyama et al. 2013). In addition, the MJO skeleton model reproduces statistics of MJO events, such as the number and duration of events, that are similar to the statistics of MJO events in nature (Stachnik et al. 2015).

While the simplified asymptotic models in this paper include several realistic aspects of tropical–extratropical interactions, some other physical mechanisms are not included. For instance, the meridional structures of the variables here are set to be the leading parabolic cylinder functions. With more complicated meridional structures, the interaction mechanism will be richer and more realistic, and it would allow the model to cope with different background states, such as the boreal summer and/or winter, when the ITCZ is off the equator. Such topics are interesting avenues for future investigations.

Acknowledgments. The research of A.J.M. is partially supported by Office of Naval Research Grant ONR MURI N00014-12-1-0912. The research of S.N.S. is partially supported by Office of Naval Research Grant ONR MURI N00014-12-1-0912, ONR Young Investigator Award ONR N00014-12-1-0744, National Science Foundation Grant NSF DMS-1209409, and a Sloan Research Fellowship. S.C. is supported as a postdoctoral research associate by the ONR grants.

APPENDIX

Asymptotic Expansion of the Meridional Truncated System

The parabolic cylinder functions that are used to define the meridional structure of the baroclinic variables are as follows:

$$\Phi_m(y) = (m!\sqrt{\pi})^{-1/2} 2^{-m/2} e^{-y^2/2} H_m(y), \quad (\text{A1})$$

with Hermite polynomials $H_m(y)$ defined by

$$H_m(y) = (-1)^m e^{y^2} \frac{d^m}{dy^m} e^{-y^2}. \quad (\text{A2})$$

The parabolic cylinder functions form an orthonormal basis on the 1D function space. The first few functions are

$$\begin{aligned}\Phi_0(y) &= \pi^{-1/4} e^{-y^2/2}, \\ \Phi_1(y) &= \pi^{-1/4} \sqrt{2} y e^{-y^2/2}, \\ \Phi_2(y) &= \pi^{-1/4} \frac{1}{\sqrt{2}} (2y^2 - 1) e^{-y^2/2}.\end{aligned}\quad (\text{A3})$$

The parabolic cylinder functions satisfy the following identities:

$$\begin{aligned}\mathcal{L}_+ \Phi_m(y) &= (2m)^{1/2} \Phi_{m-1}(y), \\ \mathcal{L}_- \Phi_m(y) &= -[2(m+1)]^{1/2} \Phi_{m+1}(y),\end{aligned}\quad (\text{A4})$$

which help to simplify many expressions, where the operators \mathcal{L}_\pm are defined as $\mathcal{L}_\pm = \partial/\partial y \pm y$.

The equations in (3) for the Walker circulation can be written for the truncated system as

$$-l_{1sx}^{(0)} + v_{1s}^{(1)} + \frac{1}{\sqrt{2}} \overline{H} a_{1s}^{(0)} = \frac{1}{\sqrt{2}} c_q \tilde{S}^x, \quad (\text{A5a})$$

$$-l_{1sx}^{(2)} = 0, \quad (\text{A5b})$$

$$r_{1sx}^{(0)} + \frac{1}{\sqrt{2}} \overline{H} a^{(0)} = \frac{1}{\sqrt{2}} c_q \tilde{S}^x, \quad (\text{A5c})$$

$$r_{1sx}^{(2)} - \sqrt{2} v_{s1}^{(1)} = 0 \quad (\text{A5d})$$

$$-l_{1s}^{(0)} + \sqrt{2} r_{1s}^{(2)} = 0, \quad (\text{A5e})$$

$$\frac{\tilde{Q}}{\sqrt{2}} (r_{1sx}^{(0)} - l_{1sx}^{(0)}) + \frac{\tilde{Q}}{\sqrt{2}} v_{1s}^{(1)} + \overline{H} a_{1s}^{(0)} = c_\theta \tilde{S}^x, \quad \text{and} \quad (\text{A5f})$$

$$\frac{\tilde{Q}}{\sqrt{2}} (r_{1sx}^{(2)} - l_{1sx}^{(2)}) - \tilde{Q} v_{1s}^{(1)} = 0. \quad (\text{A5g})$$

The solution to this system of equations is the Walker circulation in the meridional truncated system, and it can be written as

$$L^2 Y B_{3r'} - Y B_{3r'} = -L^2 Y B_{1T_2} - L^2 Y B_{2T_1} + Y B_{1x'x'r'} + \mathcal{B}_{T_3}(\mathbf{U}_{1a}, \mathbf{U}_{1a}) + \mathcal{B}_{T_3}(\mathbf{U}_{1a}, \mathbf{U}_{1W}) + \mathcal{B}_{T_3}(\mathbf{U}_{1W}, \mathbf{U}_{1W}), \quad (\text{A9a})$$

$$\mathcal{N} \mathbf{U}_{3r'} + \mathcal{L}_U \mathbf{U}_3 = -\mathbf{U}_{1T_2} - \mathbf{U}_{2T_1} + \mathbf{F}_{3U_2, U_{1a}} + \mathbf{F}_{3U_2, U_{1W}} + \mathcal{B}_3(B_1, \mathbf{U}_{1a}) + \mathcal{B}_3(B_1, \mathbf{U}_{1W}). \quad (\text{A9b})$$

Here, $\mathcal{N} = \text{diag}(1, 1, 1, 1, 0, 1, 1, 1)$ is the 8×8 matrix in which the “0” entry is to eliminate $\partial_r v^{(1)}$, \mathbf{F} represents terms from the nonlinear interactions between q and a , and \mathcal{B} represents the bilinear terms from the nonlinear interactions in the dry dynamics. The detailed descriptions for these terms can be found in Chen et al. (2015).

REFERENCES

Adames, A. F., and D. Kim, 2016: The MJO as a dispersive, convectively coupled moisture wave: Theory and observations. *J. Atmos. Sci.*, **73**, 913–941, doi:10.1175/JAS-D-15-0170.1.

$$r_{1Wx}^{(0)} = -\frac{c_q - c_\theta}{\sqrt{2}(\tilde{Q} - 1)} \tilde{S}^x, \quad (\text{A6a})$$

$$l_{1Wx}^{(0)} = \frac{\sqrt{2}(c_q - c_\theta)}{\tilde{Q} - 1} \tilde{S}^x, \quad (\text{A6b})$$

$$r_{1Wx}^{(2)} = \frac{1}{\sqrt{2}} l_{1Wx}^{(0)} \quad (\text{A6c})$$

$$v_{1W}^{(1)} = \frac{1}{2} l_{1Wx}^{(0)}, \quad (\text{A6d})$$

$$q_{1W}^{(0)} = 0, \quad \text{and} \quad (\text{A6e})$$

$$a_{1W}^{(0)} = \frac{\tilde{Q} c_q - c_\theta}{\overline{H}(\tilde{Q} - 1)} \tilde{S}^x. \quad (\text{A6f})$$

By writing the baroclinic variables as $\mathbf{U} = [l^{(0)}, l^{(2)}, r^{(0)}, r^{(2)}, v^{(1)}, q^{(0)}, q^{(2)}]$ for the truncated system, and writing $\mathbf{U}_1 = \mathbf{U}_{1a} + \mathbf{U}_{1W}$ to separate the Walker circulation \mathbf{U}_{1W} from the anomalies \mathbf{U}_{1a} , the asymptotic expansion of (1), (2), (8), (11), and (12) can be written in abstract form as follows. Expanding (1) and (2) in powers of δ , the first-order system is

$$L^2 Y B_{1r'} - Y B_{1r'} = 0, \quad (\text{A7a})$$

$$\mathcal{N} \mathbf{U}_{1a} + \mathcal{L}_U \mathbf{U}_{1a} = 0; \quad (\text{A7b})$$

the second-order system is

$$L^2 Y B_{2r'} - Y B_{2r'} = -L^2 Y B_{1T_1}, \quad (\text{A8a})$$

$$\mathcal{N} \mathbf{U}_{2r'} + \mathcal{L}_U \mathbf{U}_2 = -\mathbf{U}_{1aT_1} + \mathbf{F}_{2U_{1a}} + \mathbf{F}_{2U_{1W}}; \quad (\text{A8b})$$

and the third-order system is

Chen, S., and S. N. Stechmann, 2016: Nonlinear traveling wave solutions for MJO skeleton model. *Commun. Math. Sci.*, **14**, 571–592, doi:10.4310/CMS.2016.v14.n2.a11.

—, A. J. Majda, and S. N. Stechmann, 2015: Multiscale asymptotics for the skeleton of the Madden–Julian oscillation and tropical–extratropical interactions. *Math. Climate Wea. Forecasting*, **1**, 43–69, doi:10.1515/mcwf-2015-0003.

Ferranti, L., T. N. Palmer, F. Molteni, and E. Klinker, 1990: Tropical–extratropical interaction associated with the 30–60 day oscillation and its impact on medium and extended range prediction. *J. Atmos. Sci.*, **47**, 2177–2199, doi:10.1175/1520-0469(1990)047<2177:TEIAWT>2.0.CO;2.

- Frederiksen, J. S., and C. S. Frederiksen, 1993: Monsoon disturbances, intraseasonal oscillations, teleconnection patterns, blocking, and storm tracks of the global atmosphere during January 1979: Linear theory. *J. Atmos. Sci.*, **50**, 1349–1372, doi:10.1175/1520-0469(1993)050<1349:MDIOTP>2.0.CO;2.
- Gloekler, L. C., and P. E. Roundy, 2013: Modulation of the extratropical circulation by combined activity of the Madden-Julian oscillation and equatorial Rossby waves during boreal winter. *Mon. Wea. Rev.*, **141**, 1347–1357, doi:10.1175/MWR-D-12-00179.1.
- Hendon, H. H., and M. L. Salby, 1994: The life cycle of the Madden-Julian oscillation. *J. Atmos. Sci.*, **51**, 2225–2237, doi:10.1175/1520-0469(1994)051<2225:TLCOTM>2.0.CO;2.
- Hoskins, B. J., and F.-F. Jin, 1991: The initial value problem for tropical perturbations to a baroclinic atmosphere. *Quart. J. Roy. Meteor. Soc.*, **117**, 299–317, doi:10.1002/qj.49711749803.
- , and T. Ambrizzi, 1993: Rossby wave propagation on a realistic longitudinally varying flow. *J. Atmos. Sci.*, **50**, 1661–1671, doi:10.1175/1520-0469(1993)050<1661:RWPOAR>2.0.CO;2.
- Jin, F.-F., and B. J. Hoskins, 1995: The direct response to tropical heating in a baroclinic atmosphere. *J. Atmos. Sci.*, **52**, 307–319, doi:10.1175/1520-0469(1995)052<0307:TDRTH>2.0.CO;2.
- Khouider, B., and A. J. Majda, 2005: A non-oscillatory balanced scheme for an idealized tropical climate model. Part I: Algorithm and validation. *Theor. Comput. Fluid Dyn.*, **19**, 331–354, doi:10.1007/s00162-005-0170-8.
- Lau, W. K. M., and D. E. Waliser, Eds., 2012: *Intraseasonal Variability in the Atmosphere–Ocean Climate System*. Springer, 437 pp.
- Liebmann, B., and D. L. Hartmann, 1984: An observational study of tropical–midlatitude interaction on intraseasonal time scales during winter. *J. Atmos. Sci.*, **41**, 3333–3350, doi:10.1175/1520-0469(1984)041<3333:AOSOTI>2.0.CO;2.
- Lin, H., G. Brunet, and J. Derome, 2009: An observed connection between the North Atlantic oscillation and the Madden-Julian oscillation. *J. Climate*, **22**, 364–380, doi:10.1175/2008JCLI2515.1.
- Madden, R. A., and P. R. Julian, 1971: Detection of a 40–50 day oscillation in the zonal wind in the tropical Pacific. *J. Atmos. Sci.*, **28**, 702–708, doi:10.1175/1520-0469(1971)028<0702:DOADOI>2.0.CO;2.
- , and —, 1972: Description of global-scale circulation cells in the tropics with a 40–50 day period. *J. Atmos. Sci.*, **29**, 1109–1123, doi:10.1175/1520-0469(1972)029<1109:DOGSCC>2.0.CO;2.
- , and —, 1994: Observations of the 40–50-day tropical oscillation—A review. *Mon. Wea. Rev.*, **122**, 814–837, doi:10.1175/1520-0493(1994)122<0814:OOTDIO>2.0.CO;2.
- Majda, A. J., 2003: *Introduction to PDEs and Waves for the Atmosphere and Ocean*. Courant Lecture Notes in Mathematics, Vol. 9, American Mathematical Society, 234 pp.
- , and J. A. Biello, 2003: The nonlinear interaction of barotropic and equatorial baroclinic Rossby waves. *J. Atmos. Sci.*, **60**, 1809–1821, doi:10.1175/1520-0469(2003)060<1809:TNIOPA>2.0.CO;2.
- , and R. Klein, 2003: Systematic multiscale models for the tropics. *J. Atmos. Sci.*, **60**, 393–408, doi:10.1175/1520-0469(2003)060<0393:SMMFTT>2.0.CO;2.
- , and S. N. Stechmann, 2009: The skeleton of tropical intraseasonal oscillations. *Proc. Natl. Acad. Sci. USA*, **106**, 8417–8422, doi:10.1073/pnas.0903367106.
- , and —, 2011: Nonlinear dynamics and regional variations in the MJO skeleton. *J. Atmos. Sci.*, **68**, 3053–3071, doi:10.1175/JAS-D-11-053.1.
- , R. R. Rosales, E. G. Tabak, and C. V. Turner, 1999: Interaction of large-scale equatorial waves and dispersion of Kelvin waves through topographic resonances. *J. Atmos. Sci.*, **56**, 4118–4133, doi:10.1175/1520-0469(1999)056<4118:IOLSEW>2.0.CO;2.
- Matthews, A., and G. N. Kiladis, 1999: The tropical–extratropical interaction between high-frequency transients and the Madden-Julian oscillation. *Mon. Wea. Rev.*, **127**, 661–677, doi:10.1175/1520-0493(1999)127<0661:TTEIBH>2.0.CO;2.
- , B. J. Hoskins, and M. Masutani, 2004: The global response to tropical heating in the Madden-Julian oscillation during the northern winter. *Quart. J. Roy. Meteor. Soc.*, **130**, 1991–2011, doi:10.1256/qj.02.123.
- Ogrosky, H. R., and S. N. Stechmann, 2015: The MJO skeleton model with observation-based background state and forcing. *Quart. J. Roy. Meteor. Soc.*, **141**, 2654–2669, doi:10.1002/qj.2552.
- Ray, P., and C. Zhang, 2010: A case study of the mechanics of extratropical influence on the initiation of the Madden-Julian oscillation. *J. Atmos. Sci.*, **67**, 515–528, doi:10.1175/2009JAS3059.1.
- Roundy, P. E., 2011: Tropical–extratropical interactions. *Intraseasonal Variability in the Atmosphere–Ocean Climate System*, W. K. M. Lau and D. E. Waliser, Eds., Springer, 437 pp.
- Sobel, A., and E. Maloney, 2013: Moisture modes and the eastward propagation of the MJO. *J. Atmos. Sci.*, **70**, 187–192, doi:10.1175/JAS-D-12-0189.1.
- Stachnik, J. P., D. E. Waliser, A. J. Majda, S. N. Stechmann, and S. Thual, 2015: Evaluating MJO event initiation and decay in the skeleton model using RMM-like index. *J. Geophys. Res. Atmos.*, **120**, 486–508, doi:10.1002/2015JD023916.
- Stechmann, S. N., and H. R. Ogrosky, 2014: The Walker circulation, diabatic heating, and outgoing longwave radiation. *Geophys. Res. Lett.*, **41**, 9097–9105, doi:10.1002/2014GL062257.
- , and A. J. Majda, 2015: Identifying the skeleton of the Madden-Julian oscillation in observational data. *Mon. Wea. Rev.*, **143**, 395–416, doi:10.1175/MWR-D-14-00169.1.
- Thual, S., and A. J. Majda, 2015: A suite of skeleton models for the MJO with refined vertical structure. *Math. Climate Wea. Forecasting*, **1**, 70–95, doi:10.1515/mcfw-2015-0004.
- , and —, 2016: A skeleton model for the MJO with refined vertical structure. *Climate Dyn.*, **46**, 2773–2786, doi:10.1007/s00382-015-2731-x.
- , —, and S. N. Stechmann, 2014: A stochastic skeleton model for the MJO. *J. Atmos. Sci.*, **71**, 697–715, doi:10.1175/JAS-D-13-0186.1.
- , —, and —, 2015: Asymmetric intraseasonal events in the stochastic skeleton MJO model with seasonal cycle. *Climate Dyn.*, **45**, 603–618, doi:10.1007/s00382-014-2256-8.
- Webster, P. J., 1972: Response of the tropical atmosphere to local steady forcing. *Mon. Wea. Rev.*, **100**, 518–541, doi:10.1175/1520-0493(1972)100<0518:ROTTAT>2.3.CO;2.
- , 1981: Mechanisms determining the atmospheric response to sea surface temperature anomalies. *J. Atmos. Sci.*, **38**, 554–571, doi:10.1175/1520-0469(1981)038<0554:MDTART>2.0.CO;2.
- , 1982: Seasonality in the local and remote atmospheric response to sea surface temperature anomalies. *J. Atmos. Sci.*, **39**, 41–52, doi:10.1175/1520-0469(1982)039<0041:SITLAR>2.0.CO;2.
- Weickmann, K. M., 1983: Intraseasonal circulation and outgoing longwave radiation modes during Northern Hemisphere winter. *Mon. Wea. Rev.*, **111**, 1838–1858, doi:10.1175/1520-0493(1983)111<1838:ICAOLR>2.0.CO;2.

- , and E. Berry, 2009: The tropical Madden–Julian oscillation and the global wind oscillation. *Mon. Wea. Rev.*, **137**, 1601–1614, doi:[10.1175/2008MWR2686.1](https://doi.org/10.1175/2008MWR2686.1).
- , G. R. Lussky, and J. E. Kutzbach, 1985: Intraseasonal (30–60 day) fluctuations of outgoing longwave radiation and 250 mb streamfunction during northern winter. *Mon. Wea. Rev.*, **113**, 941–961, doi:[10.1175/1520-0493\(1985\)113<0941:IDFOOL>2.0.CO;2](https://doi.org/10.1175/1520-0493(1985)113<0941:IDFOOL>2.0.CO;2).
- Wheeler, M. C., and H. H. Hendon, 2004: An all-season real-time multivariate MJO index: Development of an index for monitoring and prediction. *Mon. Wea. Rev.*, **132**, 1917–1932, doi:[10.1175/1520-0493\(2004\)132<1917:AARMMI>2.0.CO;2](https://doi.org/10.1175/1520-0493(2004)132<1917:AARMMI>2.0.CO;2).
- Yang, D., and A. P. Ingersoll, 2013: Triggered convection, gravity waves, and the MJO: A shallow-water model. *J. Atmos. Sci.*, **70**, 2476–2486, doi:[10.1175/JAS-D-12-0255.1](https://doi.org/10.1175/JAS-D-12-0255.1).
- Yoneyama, K., C. Zhang, and C.-N. Long, 2013: Tracking pulses of the Madden–Julian oscillation. *Bull. Amer. Meteor. Soc.*, **94**, 1871–1891, doi:[10.1175/BAMS-D-12-00157.1](https://doi.org/10.1175/BAMS-D-12-00157.1).
- Zhang, C., 2005: Madden–Julian oscillation. *Rev. Geophys.*, **43**, RG2003, doi:[10.1029/2004RG000158](https://doi.org/10.1029/2004RG000158).
- , 2013: Madden–Julian oscillation: Bridging weather and climate. *Bull. Amer. Meteor. Soc.*, **94**, 1849–1870, doi:[10.1175/BAMS-D-12-00026.1](https://doi.org/10.1175/BAMS-D-12-00026.1).